

Glycomimetics

The Conformation of the Mannopyranosyl Phosphate Repeating Unit of the Capsular Polysaccharide of *Neisseria meningitidis* Serogroup A and Its Carba-Mimetic

Ilaria Calloni,^[a,b] Luca Unione,^[c] Gonzalo Jiménez-Osés,^[d] Francisco Corzana,^[d] Linda Del Bino,^[e] Alessio Corrado,^[e,f] Olimpia Pitirollo,^[f] Cinzia Colombo,^[f] Luigi Lay,^[f] Roberto Adamo,^[e] and Jesús Jiménez-Barbero*^[a,b,g]

Abstract: *Neisseria meningitidis* serogroup A (MenA) is an aerobic diplococcal Gram-negative bacterium responsible for epidemic meningitis disease. Its capsular polysaccharide (CPS) has been identified as the primary virulence factor of MenA. This polysaccharide suffers from chemical lability in water. Thus, the design and synthesis of novel and hydrolytically stable structural analogues of MenA CPS may provide additional tools for the development of therapies against this disease. In this context, the structural features of the natural phosphorylated monomer have been analyzed and compared to those of its

carba-analogue, where the endocyclic oxygen has been replaced by a methylene moiety. The lowest energy geometries of the different molecules have been calculated using a combination of quantum mechanical techniques and molecular dynamics simulations. The predicted results have been compared and validated using NMR experiments. The results indicate that the more stable designed glycomimetics may adopt the conformation adopted by the natural monomer, although they display a wider flexibility around the torsional degrees of freedom.

Introduction

Most of the cases of meningococcal disease worldwide are caused by six serogroups (A, B, C, Y, W and X). Serogroup A, in particular, has been responsible for the largest and most devastating epidemic meningitis disease in developing countries in the first part of the twentieth century.^[1] Today the meningitis epidemics caused by MenA are rare in the US and Europe and

especially afflict the sub-Saharan region of Africa.^[2] The capsular polysaccharide (CPS), which covers the bacterial cell surface, is distinct within the different serogroups and has been identified as the primary virulence factor. The CPS of serogroup A (MenA) has a backbone formed by (1→6)-linked 2-acetamido-2-deoxy- α -D-mannopyranosyl phosphate repeating units (Figure 1).^[3]

This polysaccharide suffers from poor stability of the anomeric linkage that tends to hydrolyze significantly in aqueous solutions and a high temperature (above 4 °C).^[4] The reason for this instability seems to be the presence of a phosphodiester linkage at the anomeric position together with the axially-oriented *N*-acetyl group at position 2 of the mannosamine moiety, which can assist the departure of the phosphomonoester group by facilitating the cleavage of the C1–O1 bond.^[4]

Consequently, there is an increasing interest in the design and synthesis of novel and hydrolytically stable mimetic of MenA capsular polysaccharide. The hydrolysis of the glycosidic linkage can be avoided by chemical modification of the glycosyl 1-*O*-phosphate moiety using sugar mimicry, replacing the endocyclic oxygen atom at the pyranose ring with a methylene group.^[5,6] MenA carba-analogues from monomer to trimer have been previously synthesized. Only the dimer was recognized by *anti* MenA PS antibodies^[5,7,8] and the CRM₁₉₇-conjugated trimer was the sole neo-glycoconjugate able to induce bactericidal antibodies, although at a lower level compared to a reference MenA CPS conjugate.^[5] It is well known that the three-dimensional structure of the partners plays an essential role in antigen-antibody molecular recognition processes. Herein, we de-

[a] Chemical Glycobiology Lab, CIC bioGUNE, Bizkaia Technology Park, Building 800, 48160 Derio, Spain
E-mail: jjbarbero@cicbiogune.es
<https://www.cicbiogune.es/people/jjbarbero>

[b] Department of Organic Chemistry II, Faculty of Science and Technology, University of the Basque Country, EHU-UPV, Leioa, Spain


[c] Atlas Molecular Pharma, Bizkaia Technology Park, Building 800, 48160 Derio, Spain


[d] Departamento de Química, Universidad de la Rioja, Centro Científico Tecnológico, Logroño, Spain

[e] Glycobiology Lab, GSK, Via Fiorentina 10, Siena Italy

[f] Department of Chemistry and ISTM-CNR, University of Milan, Via Golgi 19, 20133, Milan Italy

[g] Basque Foundation for Science (IKERBASQUE), 48009 Bilbao, Spain

 Supporting information and ORCID(s) from the author(s) for this article are available on the WWW under <https://doi.org/10.1002/ejoc.201801003>.

 © 2018 The Authors. Published by Wiley-VCH Verlag GmbH & Co. KGaA. This is an open access article under the terms of the Creative Commons Attribution-NonCommercial License, which permits use, distribution and reproduction in any medium, provided the original work is properly cited and is not used for commercial purposes.

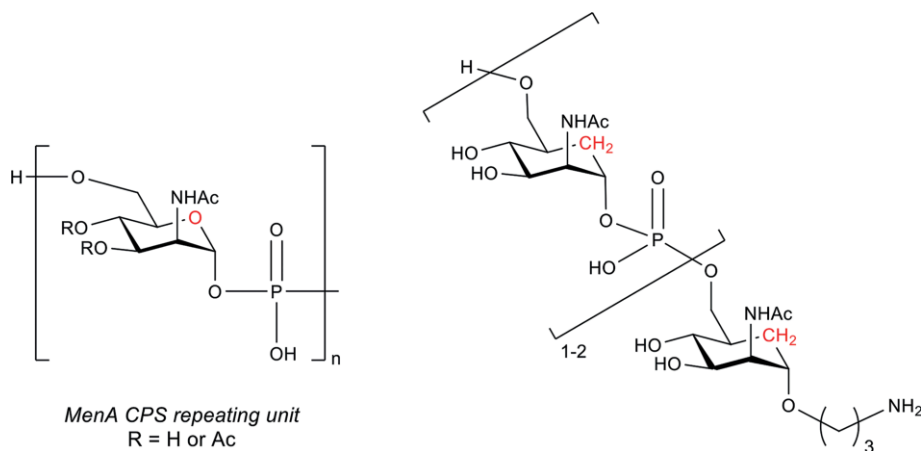


Figure 1. Natural monomer of *Neisseria meningitidis*. A capsular polysaccharide and carbasugar mimetics.^[6,7]

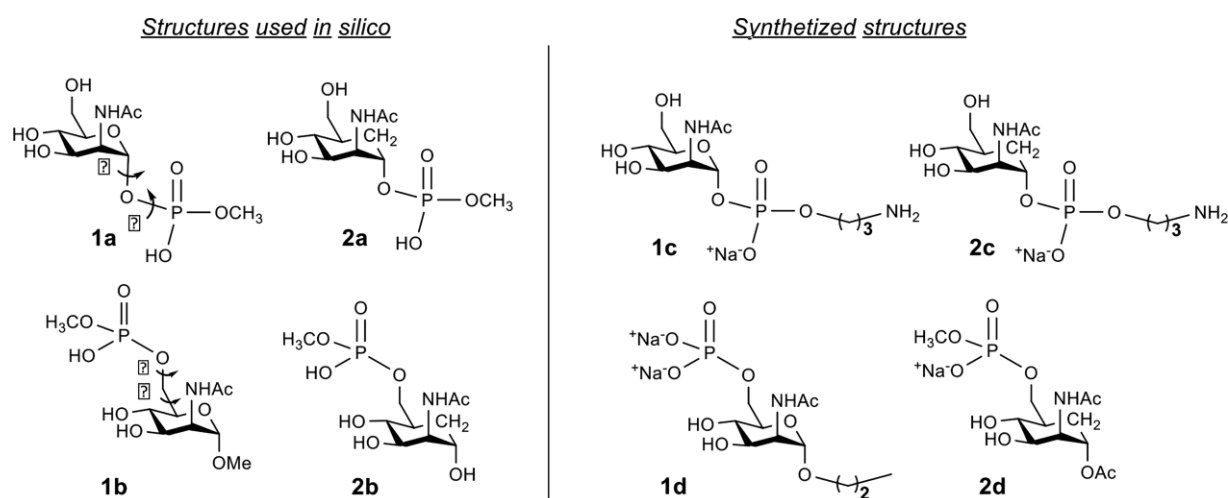


Figure 2. Schematic view of the structures of the studied compounds. Model compounds **1a** and **1b** and their C-carba glycomimetics **2a** and **2b** were subjected to *in silico* studies. Synthetic compounds **1c** and **1d** and their corresponding carba-analogues **2c** and **2d** were used for NMR studies. The torsion angles were defined as follows: $\varphi = \text{O5-C1-O-P}$ for **1a** and **1c** and $\varphi = \text{C5a-C1-O-P}$ for **2a** and **2c**, $\psi = \text{C1-O-P-OMe}$, $\omega = \text{O5-C5-C6-O6}$ for **1b** and **1d** and $\omega = \text{C5a-C5-C6-O6}$ for **2b** and **2d**, and $\theta = \text{C5-C6-O6-P}$.

scribe the conformational analysis obtained by using a combination of quantum mechanical calculations and molecular dynamics (MD) simulations of the 2-acetamido-2-deoxy- α -D-mannopyranosyl derivatives **1a** and **1b** (with a methyl phosphodiester linked at the anomeric and primary hydroxyls, respectively) and their carba glycomimetics **2a** and **2b** (Figure 2). The results have been validated by NMR experiments, performed on the synthesized monosaccharides **1c** and **1d** and their corresponding carba-analogues **2c** and **2d** (Figure 2).

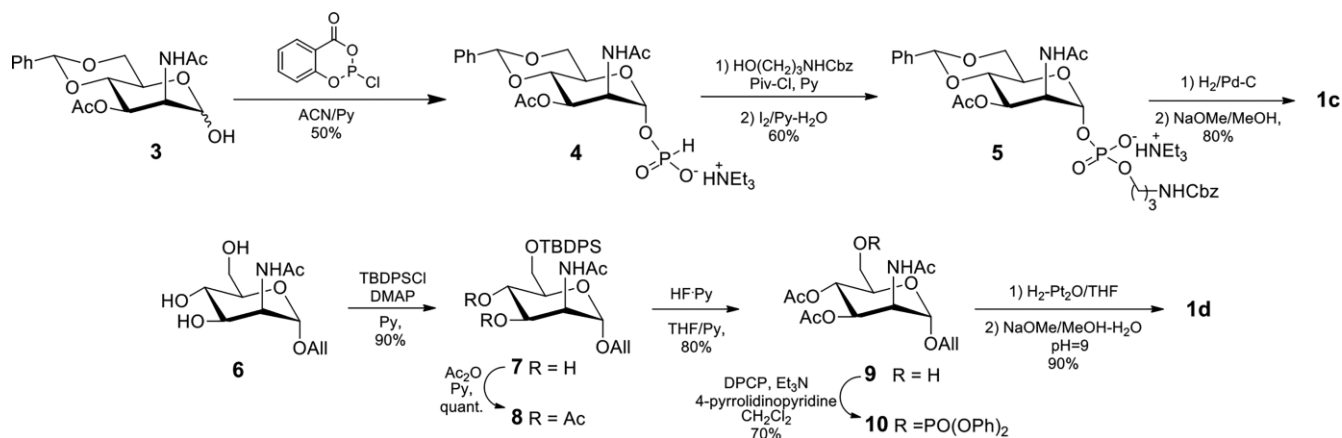
Results and Discussion

Synthesis of the Natural and Mimetic Mannosamines

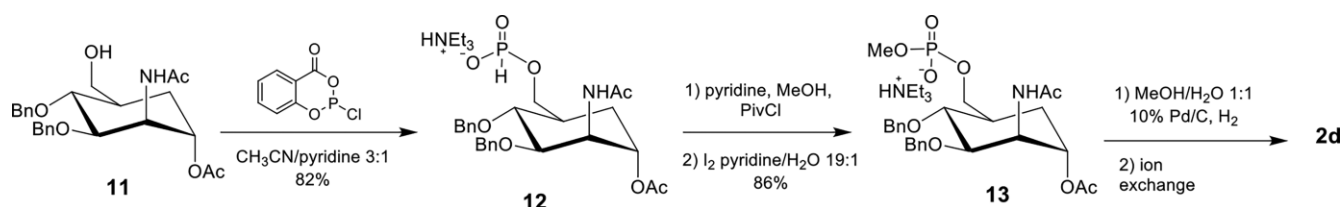
The 2-acetamido-2-deoxy- α -D-mannopyranosyl derivatives **1c**, **1d** and the carba-glycomimetics **2c**, **2d** (structurally related to **1a**, **1b** and **2a**, **2b** used in the computational studies) were synthesized according to previously reported procedures (Figure 2 and Scheme 1 and Scheme 2, see Sup Info for details).^[7,8] Mannosamine **1c** and the carba-analogue **2c** were equipped

with an α -phosphopropylamine linker in order to resemble the phosphodiester linkage present in the natural *MenA* polysaccharide. The mannosamine **1d**, structurally similar to **1b**, was synthesized with the anomeric position blocked in α -configuration by a propyl linker. The carba analogue **2d** was obtained as phosphomethyl monoester counterpart of **2b**.

The synthesis of **1c** (Scheme 1) was achieved starting from the previously reported compound **3**,^[9] which was subjected to phosphorylation of the anomeric position with 2-chloro-1,3,2-benzodioxaphosphorin-4-one, followed by condensation with benzyl *N*-(3-hydroxypropyl) carbamate to provide **5**. Hydrogenation in the presence of Pd/C and methanolysis under Zemplén conditions gave the target molecule **1c**, which was purified by size exclusion chromatography. For the synthesis of **1d** (Scheme 1), allyl mannosamine **6** was silylated at the 6-hydroxyl group and acetylated at positions 3 and 4. After removal of the *tert*-butyldiphenylsilyl protection with HF in pyridine, the resulting alcohol **9** was phosphorylated with diphenylchlorophosphate in the presence of 4-pyrrolidinopyridine/triethylamine to give **10**, which was deprotected by PtO₂-catalyzed



Scheme 1. Chemical synthesis of mannosamines **1c** and **1d**.



Scheme 2. Chemical synthesis of the carba analogue, **2d**.

hydrogenation and methanolysis to afford compound **1d**, which was chromatographed on size exclusion column.

The carba-analogue **2c** was synthesized as previously reported by Qi Gao et al. Compound **2d** was prepared starting from the previously reported intermediate **11** (Scheme 2),^[8] which was treated with 2-chloro-1,3,2-benzodioxphosphorin-4-one to obtain hydrogen phosphonate **12**. Due to its poor stability, compound **12** was promptly treated with pivaloyl chloride in pyridine and MeOH, followed by oxidation (I_2 in pyridine/water) to afford methyl phosphate **13**. Removal of benzyl ethers via Pd/C hydrogenation, followed by ion exchange with Dowex 50W-X8 resin gave the desired product **2d**, which was isolated as a sodium salt.

Conformational Analysis

The conformational behavior of different glycomimetics, including carbasugars,^[10,11] C-glycosyl compounds^[12] and other mimetics^[13,14] have been largely discussed. Their ability to mimic the binding features of the natural saccharides has also been subject of detailed investigations.^[15,16] Generally speaking, for the glycomimetics, the lack of the stereoelectronic stabilization provided by the *exo*-anomeric effect,^[17] provides additional flexibility around the glycosidic torsional angles of these molecules.^[18] Therefore, the knowledge of the geometrical and dynamic features of these molecules requires their detailed conformational analysis paying special attention to the different torsional degrees of freedom (glycosidic linkages and pendant groups) as well as the geometry of the six-membered ring. The presence of the phosphate group poses additional structural complexity of these molecules compared with natural sugars.

The conformational preferences of compounds **1a**, **1b**, **2a**, and **2b** (Figure 2) were evaluated using a combined theoretical (quantum mechanical and MD simulations) and experimental (NMR) approach. The latter was applied to the corresponding synthetic model compounds **1c**, **1d**, **2c**, and **2d**. Since **1a** is not substituted at O6, the conformation around ω and θ was studied using compound **1b** (see below).

The Conformation of the Natural Analogues **1a** and **1c** and their Carba-Mimetics, **2a** and **2c** (Anomeric Phosphates)

For compound **1a**, a long (1.5 μ s) MD simulation (Figure 3a) was performed using the GLYCAM06 force field, specific for carbohydrate molecules, using explicit solvent molecules (water) and periodic boundary conditions. The results indicate that there is a highly preferred conformation for the glycosidic linkage in terms of φ/Ψ values. As expected for a natural sugar such as **1a**, the φ value is consistent with the *exo-syn* conforma-

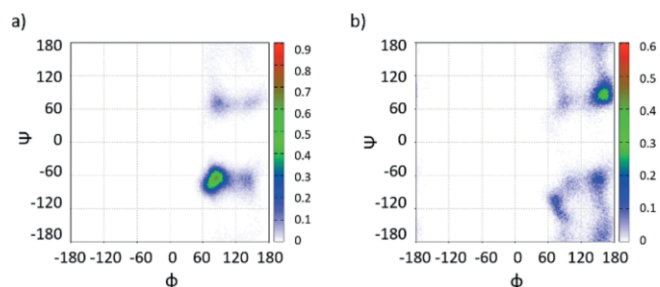


Figure 3. φ/ψ plots derived from 1.5 μ s MD simulations in explicit water for a) **1a** (GLYCAM06 force field) and b) **2a** (GAFF).

tion (Figure 4). Indeed, the stereoelectronic contribution of the *exo*-anomeric effect strongly stabilizes this geometry. For Ψ , the -60° value is largely populated. Obviously, there is certain motion around the corresponding global minimum, with minor excursions to other regions of the conformation map (Figure 3a).

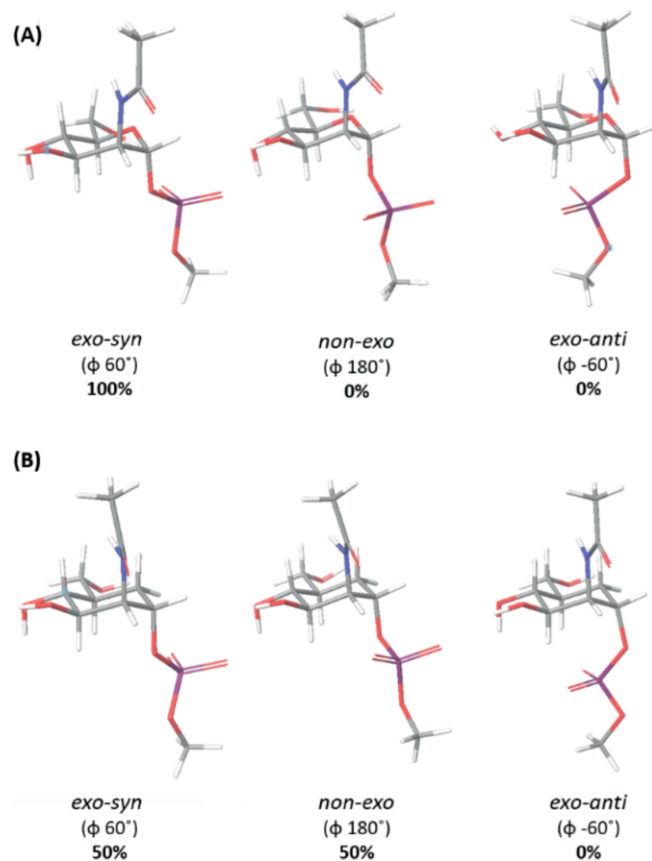


Figure 4. Representation of the *exo-syn*, *non-exo*, *exo-anti* conformers for: compound **1a** (A) and compound **2a** (B).

A similar analysis was performed with **2a**. However, in this case, the MD simulation of the carbasugar mimic, (Figure 3b) performed with the GAFF force field since GLYCAM06 does not contain parameters for carbasugars, suggested that the molecule is much more flexible, with a major contribution of the *non-exo* form, which is not present in the natural compound. There is also a larger flexibility around Ψ torsion as evidenced in Figure 3b.

The energy profile for **1a** around φ for the most stable Ψ value (-60°) was then evaluated quantum mechanically with B3LYP/6-31++G(d,p) to estimate the relative stability of the different conformers. The relative energies and derived populations calculated for the three possible staggered rotamers are given in Table 1. In agreement with the MD simulations, the *exo-syn* conformer is highly stabilized with respect to the non-exoanomeric orientation for a natural sugar **1a**, while for a carbasugar mimic **2a** the contribution of the *non-exo* form is greater. The *exo-anti* geometry, which is highly destabilized due to steric hindrance (Figure 4), presents a high level of energy for both molecules. On the other hand, the quantum mechanics

QM calculations for **2a** showed that the *exo-syn* and *non-exo* conformations display very similar energy values (Table 1).

Table 1. Relative energies (ΔE , in kcal mol $^{-1}$) and populations (% in parentheses) at 298 K between the three staggered conformations around φ : *exo-syn*, *non-exo* and *exo-anti* conformations calculated with B3LYP/6-31++g(d,p) for the natural compound **1a** and its carba-glycomimetic **2a**.

Conformation	ΔE (pop) 1a	ΔE (pop) 2a
<i>exo-syn</i>	0 (98 %)	1.5 (7 %)
<i>non-exo</i>	2.3 (2 %)	0 (93 %)
<i>exo-anti</i>	7.1 (0 %)	5.8 (0 %)

These theoretical predictions were validated through experimental NMR measurements obtained for **1c**. Different NMR experiments (^1H , $^1\text{H}\{^{31}\text{P}\}$, $^1\text{H}\text{-}^{31}\text{P}$ COSY, $^{13}\text{C}\{^1\text{H}\}$, HSQC) were performed to obtain the key NMR parameters with conformational information that could be compared to the predictions. Special attention was paid to obtain the scalar coupling constants (J) defining the conformation around φ and Ψ torsion angles (Figure 2).

In particular the $^3J_{\text{H1,P}}$, $^3J_{\text{P,C2}}$, and $^2J_{\text{P,C1}}$ values were determined (Table 2) to deduce the preferred geometry of the glycosidic linkage around φ . The comparison between the experimental J -couplings and the values calculated for the three conformations of **1a** demonstrated that the *exo-syn* conformation (Figure 4) is highly predominant for **1c** in solution. In particular, $^3J_{\text{H1,P}}$ and $^3J_{\text{C2,P}}$ showed a clear preference for this geometry. The geminal $^2J_{\text{P,C1}}$ is also consistent with a major *exo-syn* conformation.

Table 2. Theoretical (calculated for **1a**) and experimental (measured for **1c**) J couplings (in Hz) for the three staggered orientations around φ . The theoretical values were calculated through the GIAO method at the B3LYP/6-31++g(d,p) level. The agreement between the expected values for the *exo-syn* conformer and the experimental values is remarkable. See also Figure S1.

	$^3J_{\text{H1,P}}$	$^3J_{\text{P,C2}}$	$^2J_{\text{P,C1}}$
Experiment (1c)	7.7	8.9	5.5
Calculated for <i>exo-syn</i> (1a)	6.6	9.0	6.9
Calculated for <i>non-exo</i> (1a)	0.9	0.4	3.3
Calculated for <i>exo-anti</i> (1a)	19	4.2	12.3

A similar analysis was performed with the carba-analogue **2c**. The comparison between the experimental values for $^3J_{\text{H1,P}}$, $^3J_{\text{P,C2}}$, and $^2J_{\text{P,C1}}$ with those calculated quantum mechanically for the three considered conformations of **2a** (Table 3) allowed defining the population of the different conformers of **2c** in solution. Fittingly, in this case, the data supported the existence of two equal populations for the *exo-syn* and *non-exo* conformers around φ dihedral angle (Figure 4).

The estimation fully agrees with the lack of *exo*-anomeric stabilization for the carba-analogue. In the absence of stereoelectronic effects, the expected steric interactions (Figure 4 and Figure S7) are fairly similar for the two possible orientations around φ .

The Conformation of the Natural Analogues **1b** and **1d** and Their Mimetics **2b** and **2d** (C6-Phosphates)

The analysis of the 1.5 μs MD simulation performed for **1b** (Figure 5a) using the GLYCAM06 force field indicated that this com-

Table 3. Theoretical (calculated for **2a**) and experimental (measured for **2c**) J-couplings (in Hz) for the three staggered orientations around φ . The theoretical values were calculated through the GIAO method at the B3LYP/6-31++g(d,p) level. See also Figure S4.

	${}^3J_{PC,S'}$	${}^3J_{PC2}$	${}^2J_{PC1}$
Experiment (2c)	3.1	3.8	4.8
Calculated for 50 % <i>exo-syn</i> + 50 % <i>non-exo</i> (2a)	3.4	4.1	4.9
Calculated for <i>exo-syn</i> (2a)	0.5	7.5	0.6
Calculated for <i>non-exo</i> (2a)	6.3	0.8	9.2

pond is rather rigid in terms of ω/θ . As expected for a natural sugar (Scheme 3), the dominant ω value corresponds to the gauche-gauche (*gg*) conformation around C5–C6. For θ , there is a major conformation at ca. -120° , while the *anti* geometry (180°) is also present as a minor conformer, with certain flexibility around the corresponding minima (Figure 5a).

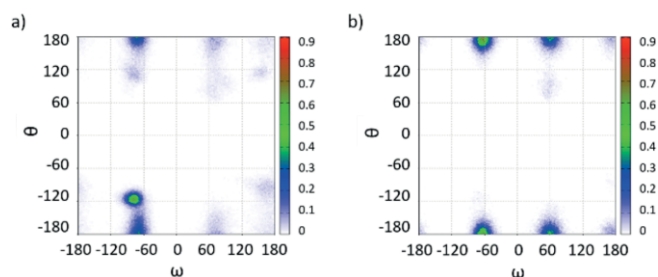
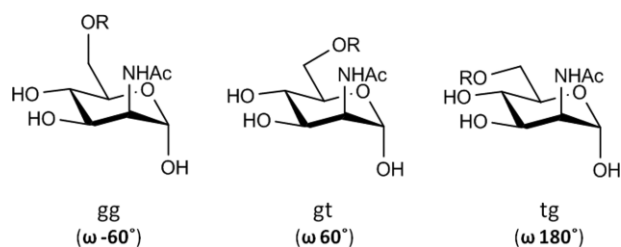


Figure 5. ω/θ plots derived from 1.5 μ s MD simulations in explicit water for a) **1b** (GLYCAM06 force field) and b) **2b** (GAFF).



Scheme 3. Schematic representation of the *gg*, *gt* and *tg* orientations around the ω dihedral angle ($\omega = O5-C5-C6-O6$) in a model α -mannosamine molecule.

The analysis of the results of the long (1.5 μ s) MD simulation for the carba-analogue **2b** (Figure 5b), performed using the GAFF force field, showed a conformational mixture of the gauche-gauche (*gg*) and gauche-trans (*gt*) orientations, with a very minor population of the trans-gauche (*tg*) conformer, as indicated by the values ω (Figure S8). However, for θ , the *anti*-geometry value is now the only populated conformational family.

The energy profile for **1b** and **2b** around ω for most stable θ value (-120° for **1b** and 180° for **2b**) was then evaluated quantum mechanically with B3LYP/6-31++g(d,p) to estimate the relative stability of the different conformers. The relative energies and derived populations calculated for the three possible stag-

gered rotamers (Figure S2 in the Supporting Information) of **1b** and carba-analogue **2b** are given in Table 4. The DFT results also support that the *gg* conformer is highly stabilized with respect to the *gt* and *tg* orientations.

Table 4. Relative energies (ΔE , in kcal mol $^{-1}$) and populations (% in parentheses) at 298 K between the 3 staggered conformations around ω : *gg*, *gt* and *tg* conformations calculated with B3LYP/6-31++g(d,p) for the natural compound **1b** and its carba-mimetic **2b**.

Conformation	ΔE [kcal/mol] 1b	ΔE [kcal/mol] 2b
<i>gg</i>	0 (100 %)	0 (100 %)
<i>gt</i>	6.2 (0 %)	4.6 (0 %)
<i>tg</i>	14.2 (0 %)	4.5 (0 %)

Again, these theoretical results obtained for natural sugar **1b** and carba-analogue **2b** were compared to those obtained through experimental NMR for compound **1d** and carba-analogue **2d**, respectively. For **1d**, in addition to the previously described NMR experiments, a J-resolved experiment was performed to get key NMR parameters with conformational information. In particular, ${}^3J_{H5,H6a}$ and ${}^3J_{H5,H6b}$ values define ω , while ${}^3J_{H6a,P}$, ${}^2J_{H6b,P}$ and ${}^3J_{C5,P}$ are related to θ torsion angle. The comparison between these experimental values with those estimated from DFT calculations for the 3 major conformers of **1b** (Table 5) allowed assessing the existence of the *gg* rotamer as the sole conformation in solution for **1d**. Regarding θ , the NMR spectroscopic data permitted to define that its major conformation corresponds to the *anti* form ($\theta = 180^\circ$), while the eclipsed one ($\theta = 120^\circ$) is also present in a minor amount.

Table 5. Theoretical (**1b**) and experimental (**1d**) J couplings for the three major orientations of ω (${}^3J_{H5,H6a,b}$) and θ (${}^3J_{H6a,6bP}$, ${}^3J_{C5,P}$) angles. The theoretical values have been calculated with B3LYP/6-31++g(d,p) basis set and GIAO method. See also Figures S2 and S3.

	${}^3J_{H5,H6a}$	${}^3J_{H5,H6b}$	
Experiment (1d)	2.1	3.1	
DFT calculation for <i>gg</i> (1b)	1.4	3.1	
DFT calculation for <i>gt</i> (1b)	1.7	8	
DFT calculation for <i>tg</i> (1b)	8.5	3.4	
	${}^3J_{H6a,P}$	${}^2J_{H6b,P}$	${}^3J_{C5,P}$
Experiment (1d)	3	4.5	7.5
Calc. for 80 % <i>anti</i> + 20 % eclipsed (1b)	3.6	4.2	7.6
Calculated for $\theta = 180^\circ$ (1b)	1.8	2.2	9
Calculated for $\theta = -120^\circ$ (1b)	11	12	2

For compound **2d**, the comparison between the experimental ${}^3J_{H5,H6a}$ and ${}^3J_{H5,H6b}$ values with those calculated quantum mechanically for **2b** (Table 6) indeed supported the theoretical predictions and suggested populations in solution of around 60 % for *gg* and 40 % for *gt* for ω , respectively (Figure 6). Regarding θ (Table 7), the experimental data permitted to define that the populations in solution are 50 % of the *anti* geometry ($\theta = 180^\circ$) and 50 % of the eclipsed one ($\theta = 120^\circ$). Therefore, the mimetic molecules are rather flexible and may show a large variety of presentations to interact with the key receptors, including those present in the natural molecules.

Table 6. Theoretical (calculated for **2b**) and experimental (measured for **2d**) J-couplings (in Hz) for the three staggered orientations around ω . The theoretical values were calculated through the GIAO method at the B3LYP/6-31++g(d,p) level. See also Figure S5.

	$^3J_{H5,H6a}$	$^3J_{H5,H6b}$
Experiment (2d)	2.7	5.2
Calculated for 60 % <i>gg</i> + 40 % <i>gt</i> (2b)	2.9	5.1
Calculated for <i>gg</i> (2b)	2.4	2.2
Calculated for <i>gt</i> (2b)	3.8	9.6
Calculated for <i>tg</i> (2b)	9.5	4

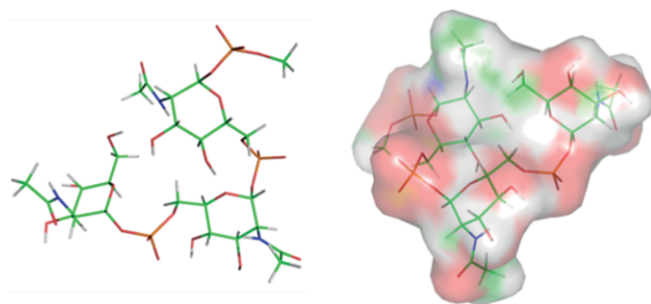


Figure 6. Different perspectives of the major conformation predicted for a natural trisaccharide, built by extension of the major *exo*-anomeric conformers found for the natural monomers. On the right handside, a surface representation is provided indicating the presentation of the polar phosphate groups (in color orange) and apolar (in color green and white) methyl moieties.

Table 7. Theoretical (calculated for **2b**) and experimental (measured for **2d**) J-couplings (in Hz) for the three staggered orientations around θ . The theoretical values were calculated through the GIAO method at the B3LYP/6-31++g(d,p) level. See also Figure S6.

	$^3J_{H6a,P}$	$^2J_{H6b,P}$	$^3J_{C5,P}$
Experiment (2d)	5	5.2	8
Calc. for 50 % eclipsed + 50 % <i>anti</i> (2b)	5	5.2	5
Calculated for θ 180 ° (2b)	2.3	< 1	7.9
Calculated for θ -120 ° (2b)	7.8	9.4	2.1

Modelling of the Carba Trimer

For the natural monosaccharide (related to **1c**), the extension of the major *exo*-anomeric geometry leads to the trisaccharide structure shown in Figure 6. In this conformation, amphipathic presentation of alternative polar and lipophilic moieties would confer to the trimer a structure compatible with a helical arrangement with a pitch of six residues (Figure 7). In particular, both the polar phosphate groups and the nonpolar methyl moieties of the acetamide substituents, responsible of this amphiphilic character, are exposed to the solvent. Therefore, this alternate presentation of polar and nonpolar patches in the trisaccharide epitope may allow it to interact with the proper receptor architecture. The non-natural carba-analogue may also present a similar geometry (Figure 8), although given the presence of non-*exo*-anomeric conformers, more extended structures might also be present (see Figure S3 in the Supporting Information). Obviously, given the higher flexibility of the non-natural oligosaccharide, the selection of the required conformer for receptor binding would impose a certain entropy penalty in the putative recognition process. However, given the small en-

ergy barriers among conformers, the unfavorable energy consequences for the use of the mimetic molecule would probably be largely overcome by the improved stability of the molecule provided by the carba motif.

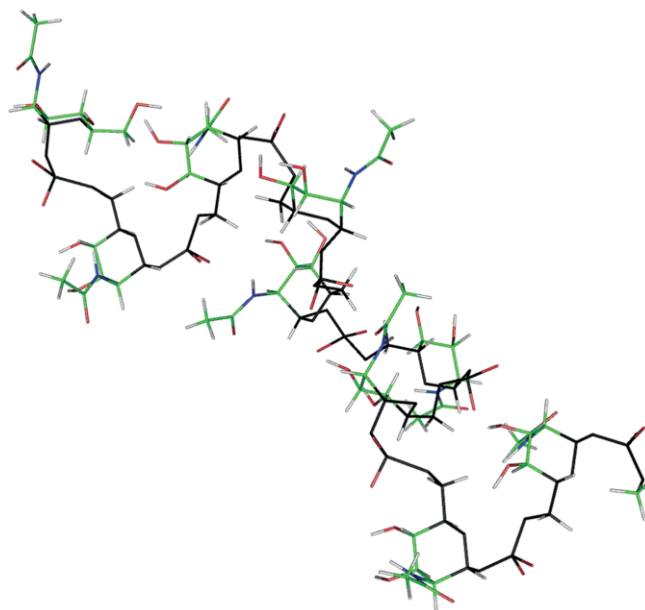


Figure 7. Schematic representation of a putative natural nonasaccharide, built by extension of the *exo*-anomeric conformer. The amphiphilic molecule adopts a helix-like structure, with a similar orientation every 6 residues. That is, the pyranose rings of 7, 8, and 9 adopt a similar presentation compared to 1, 2, and 3. In any case, the dynamic character of this structure should be highlighted.^[35]

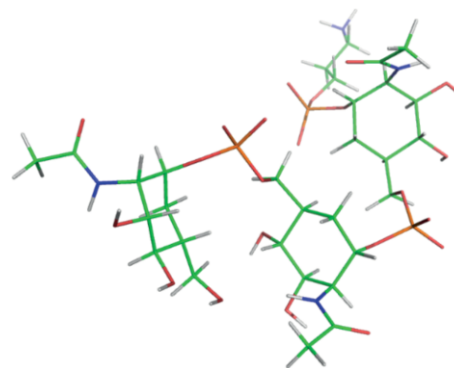


Figure 8. View of the major conformation predicted for a mimetic trisaccharide, built by extension of the *exo*-anomeric conformer. This geometry resembles that predicted for the natural molecule. Obviously, given the intrinsic flexibility of the different linkages of this molecule, the expected existence of this conformer is significantly smaller than that for the natural analogue.

Conclusions

Given the chemical and enzymatic lability of the phosphodiester linkages of the linear capsular homopolysaccharide of *Neisseria meningitidis* A, the corresponding carba analogues have been synthesized and studied as sugar mimics.^[5,7,8] In the present study, we have investigated the conformational behavior of the natural monosaccharide component of MenA CPS and

its carbasugar mimetic, by using a combination of theoretical calculations and NMR spectroscopic experiments, using the chemically synthesized 1- or 6-phosphorylated mannosamines and their carba-analogues as chemical probes. The data indicate that the natural sugar presents a well-defined conformation around the different torsional degrees of freedom, especially at the glycosidic and lateral C5–C6 chain. In addition, we have observed that, given the absence of the anomeric effect, the 1- and 6-phospho carba mannosamines display a higher conformational flexibility at the key pseudoglycosidic and aglyconic torsions compared to the native counterparts. Most importantly, one of the existing geometries corresponds to that adopted by the natural monomer. This result supports the capability of the carba mannosamine phosphate analogues to behave as conformational mimics of the natural MenA monosaccharide unit.

Experimental Section

Molecular Dynamics Simulations

The calculations were performed on **1a**, **1b**, **2a**, **2b**. Molecular Dynamics (MD) simulations were performed using the AMBER12^[19] with ff12SB and GLYCAM06^[20] force fields for the natural saccharides (**1a** and **1b**) and ff12SB and GAFF11^[21] for the carbasugar analogues (**2a** and **2b**). Long MD simulations between 500 ns and 1.5 μ s were employed to access to the conformational and dynamic information of these molecules. Additionally, MD simulations in water with the GLYCAM06 force field for performed the natural trimer and with the GAFF11 force field for the corresponding glycomimetic.

As first step, **1a** and **1b** were built using the GLYCAM carbohydrate builder web tool.^[22] The parameters and partial atomic charges for **2a** and **2b** were calculated with the antechamber module, using the GAFF force field and the AM1-BCC method for estimating the atomic charges.^[23]

The phosphate linkers were added using the xleap module of AMBER12 and the parameters and partial atomic charge were calculated with the antechamber module (derived from the DNA phosphodiester bond). Then, the resulting geometries were extensively minimized using conjugate gradients and then taken as starting structures for the MD simulations in explicit solvent. The molecules were solvated in a theoretical box of explicit TIP3P waters and the solute atoms were positioned at least at 10 Å from the solvent box edge. The equilibration phase consisted on energy minimization of the solvent followed by an energy minimization of the entire system without restraints. The system was then heated up to 300 K during 100 ps followed by 2 ns dynamics at constant temperature of 300 K, controlled by the Langevin thermostat, and constant pressure of 1 atm.

During the simulations, the SHAKE algorithm^[24] was turned on and applied to all hydrogen atoms. A cut-off of 8 Å for all nonbonded interactions was adopted. An integration time step of 2 fs was employed and periodic boundaries conditions were applied throughout. During all simulations, the particle mesh Ewald (PME) method was used to compute long-range electrostatic interactions.^[25–28] Minimization, equilibration and production phases were carried out by the pmemd.cuda^[29–31] module of AMBER 12, while the analyses of the simulations were performed using cpptraj module from AMBERTOOLS 12. Data processing and 2D plots were carried out using GNUplot software.

Quantum Mechanical Calculations: The Gaussian 09 program^[32] as used for all DFT calculations. Geometries were optimized using the B3LYP^[33,34] functional and the 6-31++g(d,p) basis set with the IEF-PCM implicit solvent model. Electronic energies were used to derive the energy profiles around different dihedral angles of interest (φ , ψ , and θ) Scalar coupling constants were computed for all the possible conformations (*exo-syn*, *non-exo*, and *exo-anti* around φ and *gg*, *gt*, and *tg* around ω) using the GIAO method.

NMR Spectroscopic Experiments: All NMR spectroscopic data were acquired at 300 K with Avance 600 MHz spectrometers (Bruker) equipped with BBI probes. NMR samples (5 mm) were prepared in the sodium phosphate buffer (20 mM, pH 7.0) in D₂O. Spectra were processed and analyzed with TOPSPIN 2.0 (Bruker) software.

Acknowledgments

This work has received funding from the Horizon 2020 research and innovation programme of the European Union under the Marie Skłodowska-Curie grant agreement Glycovax No 675671; O. P. is a student at the University of Milan and participates in a post graduate studentship program at GSK. MINECO for Grant CTQ2015-64597-C2-1P and for the Severo Ochoa Excellence Accreditation (SEV-2016-0644). We also thank MINECO (projects CTQ2015-67727-R to F. C., CTQ2015-70524-R and RYC-2013-14706 to G. J. O., CTQ2015-64597-C2-1P to J. J.-B. and SEV-2016-0644 to C. I. C. bioGUNE).

Keywords: Glycomimetics · Synthesis design · Conformation analysis · Structure elucidation · Natural products

- [1] L. K. K. Tan, G. M. Carlone, R. Borrow, *N. Eng. J. Med.* **2010**, *362*, 1511–20.
- [2] N. G. Roupheal, D. S. Stephens, *Methods Mol. Biol.* **2012**, *799*, 1–20.
- [3] D. R. Bundle, I. C. P. Smith, H. J. Jennings, *J. Biol. Chem.* **1974**, *249*, 2275–2281.
- [4] F. Berti, M. R. Romano, F. Micoli, V. Pinto, E. Cappelletti, M. Gavini, D. Proietti, G. Pluschke, C. A. MacLennan, P. Costantino, *Vaccine* **2012**, *30*, 6409–6415.
- [5] Q. Gao, M. Tontini, G. Brogioni, A. Nilo, S. Filippini, C. Harfouche, L. Polito, M. R. Romano, P. Costantino, F. Berti, R. Adamo, L. Lay, *ACS Chem. Biol.* **2013**, *8*, 2561–2567.
- [6] S. Fallarini, B. Buzzi, S. Giovarruscio, L. Polito, G. Brogioni, M. Tontini, F. Berti, R. Adamo, L. Lay, G. Lombardi, *ASC Infect. Dis.* **2015**, *1*, 487–496.
- [7] L. Toma, L. Legnani, A. Rencurosi, L. Poletti, L. Lay, G. Russo, *Org. Biomol. Chem.* **2009**, *7*, 3734.
- [8] Q. Gao, C. Zaccaria, M. Tontini, L. Poletti, P. Costantino, L. Lay, *Org. Biomol. Chem.* **2012**, *10*, 6673.
- [9] T. Fiebig, F. Freiberger, V. Pinto, M. R. Romano, A. Black, C. Litschko, A. Bethe, D. Yashunsky, R. Adamo, A. Nikolaev, F. Berti, R. Gerardy-Schahn, *J. Biol. Chem.* **2014**, *289*, 19395–19407.
- [10] V. Bordonni, V. Porkolab, S. Sattin, M. Thépaut, I. Frau, L. Favero, P. Crotti, A. Bernardi, F. Fieschi, V. Di Bussolo, *RSC Adv.* **2016**, *6*, 89578–89584.
- [11] M. Thépaut, C. Guzzi, I. Sutkeviciute, S. Sattin, R. Ribeiro-Viana, N. Varga, E. Chabrol, J. Rojo, A. Bernardi, J. Angulo, P. M. Nieto, F. Fieschi, *J. Am. Chem. Soc.* **2013**, *135*, 2518–29.
- [12] J. F. Espinosa, F. J. Cañada, J. L. Asensio, M. Martín-Pastor, H. Dietrich, M. Martín-Lomas, R. R. Schmidt, J. Jiménez-Barbero, *J. Am. Chem. Soc.* **1996**, *118*, 10862–10871.
- [13] F. Peri, J. Jiménez-Barbero, V. García-Aparicio, I. Tvaroška, F. Nicotra, *Chem. Eur. J.* **2004**, *10*, 1433–1444.
- [14] J. L. Asensio, F. J. Cañada, A. García-Herrero, M. T. Murillo, A. Fernández-Mayoralas, B. A. Johns, J. Kozak, Z. Zhu, C. R. Johnson, J. Jiménez-Barbero, *J. Am. Chem. Soc.* **1999**, *121*, 11318–11329.

- [15] I. Sutkeviciute, M. Thépaut, S. Sattin, A. Berzi, J. McGeagh, S. Grudinin, J. Weiser, A. Le Roy, J. J. Reina, J. Rojo, M. Clerici, A. Bernardi, C. Ebel, F. Fieschi, *ACS Chem. Biol.* **2014**, *9*, 1377–1385.
- [16] A. García-Herrero, E. Montero, J. L. Muñoz, J. F. Espinosa, A. Vián, J. L. García, J. L. Asensio, F. J. Cañada, J. Jiménez-Barbero, *J. Am. Chem. Soc.* **2002**, *124*, 4804–4812.
- [17] B. Xu, L. Unione, J. Sardinha, S. Wu, M. Ethève-Quellejeu, A. Pilar Rauter, Y. Blériot, Y. Zhang, S. Martín-Santamaría, D. Díaz, J. Jiménez-Barbero, M. Sollogoub, *Angew. Chem. Int. Ed.* **2014**, *53*, 9597–602; *Angew. Chem.* **2014**, *126*, 9751.
- [18] J. L. Asensio, F. J. Cañada, X. Cheng, N. Khan, D. R. Mootoo, J. Jiménez-Barbero, *Chem. Eur. J.* **2000**, *6*, 1035–1041.
- [19] D. A. Case, T. A. Darden, T. E. Cheatham, III, C. L. Simmerling, J. Wang, R. E. Duke, R. Luo, R. C. Walker, W. Zhang, K. M. Merz, B. Roberts, S. Hayik, A. Roitberg, G. Seabra, J. Swails, A. W. Götz, I. Kolossváry, K. F. Wong, F. Paesani, J. Vanicek, R. M. Wolf, J. Liu, X. Wu, S. R. Brozell, T. Steinbrecher, H. Gohlke, Q. Cai, X. Ye, J. Wang, M.-J. Hsieh, G. Cui, D. R. Roe, D. H. Mathews, M. G. Seetin, R. Salomon-Ferrer, C. Sagui, V. Babin, T. Luchko, S. Gusarov, A. Kovalenko, and P. A. Kollman (**2012**), AMBER 12, University of California, San Francisco.
- [20] K. N. Kirschner, A. B. Yongye, S. M. Tschampel, J. Gonzalez-Outeirino, C. R. Daniels, B. L. Foley, R. J. Woods, *J. Comput. Chem.* **2008**, *29*, 622–55.
- [21] J. Wang, R. M. Wolf, J. W. Caldwell, P. A. Kollman, D. A. Case, *J. Comput. Chem.* **2004**, *25*, 1157–74.
- [22] GLYCAM Carbohydrate Builder web tool. Woods Group. (**2005–2017**) GLYCAM Web. Complex Carbohydrate Research Center, University of Georgia, Athens, GA. <http://glycam.org>.
- [23] A. Jakalian, D. B. Jack, C. I. Bayly, *J. Comput. Chem.* **2002**, *23*, 1623–41.
- [24] S. Miyamoto, P. A. Kollman, *J. Comput. Chem.* **1992**, *13*, 952–962.
- [25] T. Darden, D. York, L. Pedersen, *J. Chem. Phys.* **1993**, *98*, 10089–10092.
- [26] U. Essmann, L. Perera, M. L. Berkowitz, T. Darden, H. Lee, L. G. Pedersen, *J. Chem. Phys.* **1995**, *103*, 8577–8593.
- [27] M. Crowley, T. Darden, I. T. Cheatham, I. D. Deerfield, *J. Supercomput.* **1997**, *11*, 255–278.
- [28] R. P. Laurence, H. Gerhard (Eds.), *Simulation and Theory of Electrostatic Interactions in Solution: Computational Chemistry, Biophysics and Aqueous Solutions*, American Institute of Physics, **1999**, p. 534.
- [29] S. Le Grand, A. W. Götz, R. C. Walker, *Comput. Phys. Commun.* **2013**, *184*, 374–380.
- [30] A. W. Götz, M. J. Williamson, D. Xu, D. Poole, S. Le Grand, R. C. Walker, *J. Chem. Theory Comput.* **2012**, *8*, 1542–1555.
- [31] R. Salomon-Ferrer, A. W. Götz, D. Poole, S. Le Grand, R. C. Walker, *J. Chem. Theory Comput.* **2013**, *9*, 3878–3888.
- [32] M. J. Frisch, G. W. Trucks, H. B. Schlegel, G. E. Scuseria, M. A. Robb, J. R. Cheeseman, G. Scalmani, V. Barone, B. Mennucci, G. A. Petersson, H. Nakatsuji, M. Caricato, X. Li, H. P. Hratchian, A. F. Izmaylov, J. Bloino, G. Zheng, J. L. Sonnenberg, M. Hada, M. Ehara, K. Toyota, R. Fukuda, J. Hasegawa, M. Ishida, T. Nakajima, Y. Honda, O. Kitao, H. Nakai, T. Vreven, J. A. Montgomery Jr., J. E. Peralta, F. Ogliaro, M. Bearpark, J. J. Heyd, E. Brothers, K. N. Kudin, V. N. Staroverov, R. Kobayashi, J. Normand, K. Raghavachari, A. Rendell, J. C. Burant, S. S. Iyengar, J. Tomasi, M. Cossi, N. Rega, J. M. Millam, M. Klene, J. E. Knox, J. B. Cross, V. Bakken, C. Adamo, J. Jaramillo, R. Gomperts, R. E. Stratmann, O. Yazyev, A. J. Austin, R. Cammi, C. Pomelli, J. W. Ochterski, R. L. Martin, K. Morokuma, V. G. Zakrzewski, G. A. Voth, P. Salvador, J. J. Dannenberg, S. Dapprich, A. D. Daniels, Ö. Farkas, J. B. Foresman, J. V. Ortiz, J. Cioslowski, D. J. Fox, *Gaussian 09, Revision A.02*, Gaussian, Inc., Wallingford CT, **2016**.
- [33] D. Axel, J. Becke, *Chem. Phys.* **1993**, *98*, 5648.
- [34] M. Cossi, V. Barone, R. Cammi, J. Tomasi, *Chem. Phys. Lett.* **1996**, *255*, 327–335.
- [35] J. Hložek, M. M. Kuttel, N. Ravenscroft, *Carbohydr. Res.* **2018**, *465*, 44–51.

Received: June 28, 2018